EPJ manuscript No.
(will be inserted by the editor)

Charmed meson rescattering in the reaction $\bar{p}d \to \bar{D}DN$

J. Haidenbauer[1], G. Krein[2], Ulf-G. Meißner[1,3], and A. Sibirtsev[1,3]

[1] Forschungszentrum Jülich, Institut für Kernphysik, D-52425 Jülich, Germany
[2] Instituto de Física Teórica, Universidade Estadual Paulista, Rua Pamplona, 145 - 01405-900 São Paulo, SP, Brazil
[3] Helmholtz-Institut für Strahlen- und Kernphysik (Theorie), Universität Bonn, Nußallee 14-16, D-53115 Bonn, Germany

Received: date / Revised version: date

Abstract. We examine the possibility to extract information about the DN and $\bar{D}N$ interactions from the $\bar{p}d \to D^0 D^- p$ reaction. We utilize the notion that the open-charm mesons are first produced in the annihilation of the antiproton on one nucleon in the deuteron and subsequently rescatter on the other (the spectator) nucleon. The latter process is then exploited for investigating the DN and $\bar{D}N$ interactions. We study different methods for isolating the contributions from the $D^0 p$ and $D^- p$ rescattering terms.

PACS. 13.60.Le Meson production – 14.40.Lb Charmed mesons – 25.10.+s Nuclear reactions involving few-nucleon systems – 25.43.+t Antiproton-induced reactions

1 Introduction

The distortion of charm in nuclear matter remains an heavily discussed issue since the first proposals [1] to use charmonia and open charm as a probe of the early stage of heavy-ion collisions, for a review see [2]. It was expected [3] that charmed final-state interactions (FSI) either at the partonic or the hadronic rescattering level would not distort the spectra initially produced in heavy-ion collisions, because the cross sections for any such (elastic and inelastic) scattering processes are sufficiently small. Furthermore, gluon radiation or bremsstrahlung [4–6], which distorts the original charm spectrum as well, becomes the dominant energy loss mechanism only if the heavy charmed quarks are ultra-relativistic. That is similar to the bremsstrahlung losses of electrons passing through a hydrogen target [7,8]. However, in the present experiments a large fraction of the heavy quarks are produced with momenta less than their mass and therefore the radiation losses might be negligible. In that case the heavy charmed quarks and antiquarks and, specifically, the finally detected D and $\bar{D}$ mesons are presumably not distorted in the nuclear environment and thus can probe the initial stage of the interaction, possibly, the Quark Gluon Plasma.

On the other hand it was argued [8–11] that the two basic processes involved in the energy-loss mechanism of charmed particles moving in nuclear matter, namely gluon radiation and elastic scattering, might be equally important and non-negligible. Only recently the situation changed due to the PHENIX and STAR experiments [12–15] at the Relativistic Heavy Ion Collider (RHIC). These new measurements indicate a substantial suppression of the production of open-charm mesons with transverse momenta above $\simeq$1 GeV/c from central Au+Au collisions, as compared to that from d+Au collisions. This observation could not be assigned to gluon radiation of charm and thus indirectly points to an importance of distortions due to the FSI.

Apparently, the interactions of charmed quarks or antiquarks in nuclear matter are not the same as the interactions of open-charm mesons. However, it is clear that a reasonable understanding of elastic scattering involving particles with charm on a hadronic level is highly important. While one could not measure directly the interaction of the charmed and light quarks and antiquarks, the DN and $\bar{D}N$ interactions can be studied experimentally. These could serve as a basis to construct phenomenologically the charmed FSI at the partonic rescattering level.

The basic problem is the complete lack of relevant experimental data. This situation is expected to change with the operation of the Facility for Antiproton and Ion Research (FAIR) at Darmstadt (Germany). The Proton ANtiproton at DArmstadt (PANDA) Collaboration [16] intends to investigate the distortion of open-charm mesons [17–19] in *matter* and in the *vacuum*. The *matter* measurements are based on D and $\bar{D}$ meson production in antiproton annihilation on different nuclei in order to study the A-dependence. The *vacuum* measurements explore the production of open-charm mesons by annihilating antiprotons on the deuteron and, through the rescattering of the produced D and $\bar{D}$ mesons on the spectator nucleon, the interaction in the DN and $\bar{D}N$ systems.

In the present paper we examine the possibility to extract information about the DN and $\bar{D}N$ interactions from the $\bar{p}d \to D^0 D^- p$ reaction. The study is based on the notion that those open-charm mesons are first produced by annihilating the antiproton on one of the nucleons in the deuteron and subsequently rescatter on the other (the

spectator) nucleon. The latter process is then exploited for investigating the DN and $\bar{D}N$ interactions.

To explore the potential of pertinent experiments we perform concrete calculations taking into account the nucleon exchange Born diagram, corresponding to the elementary $\bar{N}N \to \bar{D}D$ annihilation process, cf. Fig. 1a), as well as rescattering diagrams involving the DN and the $\bar{D}N$ interactions, see Fig. 1b). For those interactions we employ realistic $\bar{D}N \to \bar{D}N$ [20] and $DN \to DN$ [21] scattering amplitudes. This is a substantial improvement as compared to previous studies [22–24] which relied on rather simple assumptions as far as the DN and $\bar{D}N$ scattering amplitudes were concerned.

The paper is structured in the following way: In the subsequent section we introduce briefly the formalism used for calculating the reaction $\bar{p}d \to D^0 D^- p$. The utilized interaction models in the $\bar{D}N$ and DN channels are introduced and discussed in Sect. 3. In particular, we present results for total and differential cross sections for the various charge channels. In Sect. 4 a short overview on our present knowledge on the elementary $\bar{N}N \to \bar{D}D$ reaction is given. Our results for the reaction $\bar{p}d \to D^0 D^- p$ are shown in Sect. 5. Here the emphasis is put on the exploration of different methods for detecting and isolating the contributions from the $D^0 p$ and $D^- p$ rescattering terms. For that purpose we consider the spectator momentum distribution, Dalitz plots, the missing mass of the exchanged meson and correlations between properly defined scattering planes. The paper ends with a brief summary. As a test of our approach we also apply it to multipion production in $\bar{p}d$ annihilation and we compare our results with data available for the $\bar{p}d \to \pi^+ 2\pi^- p$ and $\bar{p}d \to 2\pi^+ 3\pi^- p$ reactions. Those results are included in an appendix.

2 Formalism

In this section we introduce the formalism we use to investigate the effects of the DN and $\bar{D}N$ interactions in antiproton annihilation on the deuteron.

Fig. 1 illustrates processes contributing to the reaction $\bar{p}d \to D\bar{D}N$. The diagrams of interest are the nucleon exchange Born diagram, Fig. 1a), and the meson rescattering diagram, Fig. 1b). The corresponding amplitudes will be denoted below by T_a and T_b, respectively.

In what follows we assume for convenience that the spectator nucleon – the nucleon that does not enter the annihilation vertices – is the proton. The case of a neutron as spectator can be treated in a similar manner. The nucleon exchange Born diagram, Fig.1a), leads to the well-known reaction amplitude [25–27]

$$T_a = \psi_d(p_s)\, T_A, \tag{1}$$

where $\psi_d(p_s)$ is the momentum-space deuteron wave function, with $\boldsymbol{p}_s$ being the proton spectator momentum, and T_A is the amplitude for the $\bar{p}n \to D^- D^0$ annihilation process. After summation over spin states the squared amplitude is given as

$$|T_a|^2 = [u(p_s)^2 + w(p_s)^2]|T_A|^2, \tag{2}$$

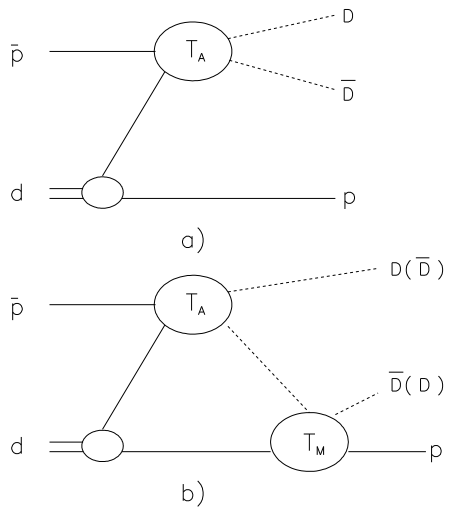

Fig. 1. Contributions to the reaction $\bar{p}d \to D\bar{D}N$: a) The Born (nucelon exchange) diagram. T_A denotes the annihilation amplitude. b) Meson rescattering diagram. T_M denotes the meson-nucleon scattering amplitude. Note that both DN and $\bar{D}N$ scatterings contribute to the reaction amplitude.

where u and w stand for the s- and d-wave components of the deuteron wave function. The overall size of the nucleon exchange contribution in Fig. 1a) is determined by the annihilation amplitude T_A, which depends on the meson channels produced in the $\bar{p}n$ annihilation. On the other hand, the spectator momentum distribution is governed predominantly by the deuteron wave function, as indicated in Eq. (2), provided that T_A is a slowly varying function of the energy.

Next we consider the rescattering diagram of Fig. 1b) where one of the mesons produced at the annihilation vertex is scattered off the spectator nucleon. In general, the intermediate meson in this diagram is not necessarily the same as the final rescattered meson. It could be an intermediate D^* vector-meson, for example. Thus, in principle a sum over all possible intermediate states is required. But in the following let us regard explicitly the features of the rescattering mechanism involving elastic $Mp \to Mp$ scattering only. Note that the formalism can be easily extended to other, non-diagonal transitions. We average over the spins in the annihilation and scattering vertices and take into account only the s-wave component $u(p_s)$ of the deuteron wave function. The d-wave component is expected to play a much less important role for the rescattering contribution [27,28] and, therefore, we ignore it here in this exploratory study. The integration for the rescattering diagram runs over the three momentum of the spectator proton in the loop and can be split into on-shell and off-shell parts, which we denote by T_b^{on} and T_b^{off}. The on-shell part is defined by taking the intermediate proton to be on-shell and is given as [27,29–32]

$$T_b^{on} = -\frac{i}{32\pi|\boldsymbol{p}|}\int_{q_-}^{q_+} dq\, u(q)\frac{q}{E_q}\, T_M\; T_A, \tag{3}$$

where T_M is the meson-proton scattering amplitude, q is the internal proton loop momentum, $E_q = (q^2 + m_p^2)^{1/2}$ with m_p the proton mass, and $\boldsymbol{p}$ is the sum of the momenta of the final proton and the rescattered meson. The limits of the integral are given by [33]

$$q_\pm = \frac{|\boldsymbol{p}|}{s_{Mp}^{1/2}}\, E^* \pm \frac{E}{s_{Mp}^{1/2}}\, p^*, \tag{4}$$

where $E{=}E_M{+}E_p$ is the sum of the energies of the final proton and the rescattered meson, while $s_{Mp}^{1/2} = (E^2{-}p^2)^{1/2}$ is their invariant energy and

$$p^{*2} = \frac{(s_{Mp} - m_p^2 - m_M^2)^2 - 4m_p^2 m_M^2}{4s_{Mp}},$$
$$E^* = \sqrt{p^{*2} + m_p^2}, \tag{5}$$

with m_M the meson mass. The evaluation of T_b requires the knowledge of both amplitudes T_M and T_A within the range of q_- to q_+ allowed for the considered reaction.

The effect of the off-shell part of the rescattering integral was investigated in detail in Refs. [27,29–31,34,35]. In those studies it was found that the shape of the spectator momentum distribution, as given by the on-shell part, remains essentially unchanged when the off-shell contribution is added. At the same time, the magnitude of the off-shell contribution is significant and can lead to modifications of the on-shell results in the order of 30% or more, but depends strongly on the specific off-shell behaviour of the annihilation and scattering amplitudes. Explicitly, the off-shell part of the amplitude can be written as [27,31, 34]

$$T_b^{off} = \frac{1}{32\pi^2 p} \int_0^\infty dq\, u(q) \frac{q}{E_q}\, T_M\; T_A \times \ln \left| \frac{E_M{+}E_p{-}E_q{-}E_-}{E_M{+}E_p{-}E_q{-}E_+} \right|, \tag{6}$$

with

$$E_\pm^2 = (p \pm q)^2 + m_{ex}^2, \tag{7}$$

where m_{ex} is the mass of the exchanged meson. In the present exploratory study we do not take into account those off-shell contributions. We stress again that these are highly model-dependent in any case.

Let us emphasize the general features of the reaction. It is clear that the spectator proton momentum spectrum is sensitive to the reaction mechanism. The nucleon exchange Born term $|T_a|^2$, given by Eq. (2), produces low and high momentum components, where the high momentum part of the spectator distribution is dominated by $w(q)$, the d-wave component of the deuteron wave function. The d-wave component is more strongly model dependent and, therefore, the corresponding contribution of the Born term to the high momentum part of the spectator distribution is afflicted with some uncertainties. However, any really significant enhancement in that spectator distribution with respect to the results based on the Born term can be definitely attributed to meson rescattering processes on the spectator. Since the scattering amplitude T_b is directly proportional to the $Mp{\to}Mp$ amplitude T_M and the annihilation amplitude T_A enters both the Born and rescattering diagrams, the enhancement in the high momentum part of the spectator distribution is related to the relative magnitudes of their contributions and, thus, essentially driven by the scattering amplitude T_M.

In any case, the isolation of the effects of T_M from the data is by no means a trivial task. There are also uncertainties related to possible contributions from other processes besides those considered above, as well as uncertainties related to the evaluation of off-shell corrections to the scattering amplitude beyond Eq. (6). Nonetheless, the situation is still manageable since those uncertainties can be kept under control to some extent by selecting carefully the reaction kinematics – see for example Ref. [36].

Our predictions for the $\bar{p}d{\to}D\bar{D}N$ reaction are presented and thoroughly discussed in Section 5. In the Appendix we illustrate the applicability of the formalism to the proton spectator distributions as measured in the $\bar{p}d{\to}\pi^+2\pi^-p$ and $\bar{p}d{\to}2\pi^+3\pi^-p$ reactions. Besides providing support for the reliability of the approach adopted for the present investigation, those results are also useful for revealing similarities but also differences in the utilization of the reaction $\bar{p}d \to nMN$ for exploring the MN interaction for different mesons and/or different kinematical regimes.

All calculations are done with the deuteron wave function of the CD-Bonn NN potential [37]. But for shedding light on the model dependence we also emply the wave functions of the Paris [38] and full Bonn [39] NN potentials. We ignore the effects of the Coulomb interaction in this exploratory study. Furthermore, we use averaged masses. Specifically, we use $m_D = 1866.9$ MeV for the mass of the D and $\bar{D}$ mesons.

3 The $\bar{D}N$ and DN interactions

Considering charm and charge conservation antiproton-deuteron annihilation allows to study the following D-meson production reactions

$$\bar{p}d \to D^0 \bar{D}^0 n, \tag{8}$$
$$\bar{p}d \to D^+ D^- n, \tag{9}$$
$$\bar{p}d \to D^0 D^- p\,. \tag{10}$$

They involve the $\bar{D}N$ as well as the DN scattering amplitude. Here we investigate only the $\bar{p}d{\to}D^0D^-p$ reaction. We select this channel because, in principle, all final particles can be measured for this reaction, which implies that there should be less uncertainties in the data evaluation discussed in the present study. For example, in case of the neutron as the spectator one needs to use the missing mass reconstruction technique. In this context let us

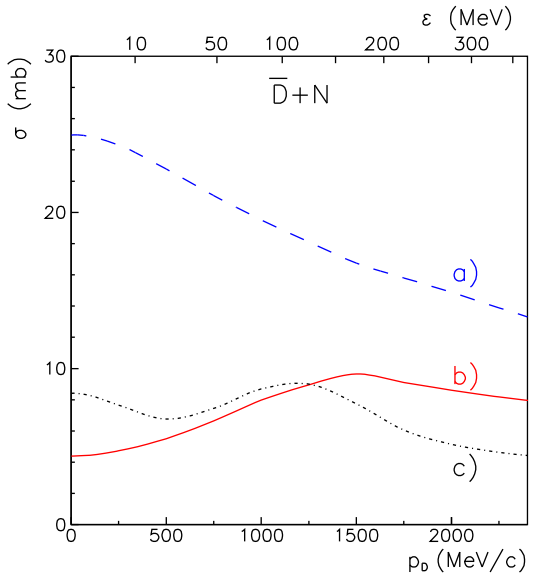

Fig. 2. Reaction cross section for (a) $D^-n \to D^-n$ (dashed line), (b) $D^-p \to D^-p$ (solid line) and (c) $D^-p \to \bar{D}^0n$ (dash-dotted line) as a function of the $\bar{D}$-meson momentum (lower axis) and the kinetic energy ϵ in the center-of-mass system (cms) (upper axis).

also recall that charged open-charm mesons are in general reconstructed by the leptonic, semileptonic and hadronic $K\pi\pi$ and $K\pi\pi\pi$ decay modes. Usually the neutral open-charm mesons can be well detected by their hadronic $D^0 \to K^-\pi^+$ and $\bar{D}^0 \to K^+\pi^-$ decays [7]. For the full reconstruction of the final state of the $\bar{p}d \to \bar{D}^0D^-p$ reaction it is therefore important that both semileptonic and hadronic modes are detected with high accuracy. This should be kept in mind for the design of future experiments, e.g., of the PANDA experiment [16]. High accuracy is crucial for identification of DN and $\bar{D}N$ rescattering effects, whose absolute values and energy dependences could be very different, as indicated by several studies using different models [22,40–44], and as will become clear from the present work, too. The identification of the different effects might be possible when a full reconstruction of the final state is feasible.

3.1 The $\bar{D}N$ amplitude

For the $\bar{D}N$ scattering amplitude we use the results of our recently published potential model [20]. This model for the $\bar{D}N$ interaction was constructed within the meson-exchange framework, but supplemented with a short-distance contribution from one-gluon-exchange. The model was developed in close analogy to the meson-exchange KN interaction of the Jülich group [45,46] utilizing SU(4) symmetry constraints. The main ingredients of the interaction are provided by vector meson (ρ, ω) exchange and higher-order box diagrams involving $\bar{D}^*N$, $\bar{D}\Delta$, and $\bar{D}^*\Delta$ intermediate states. The short range part is supplemented by additional contributions from genuine quark-gluon processes [47,48]. The reaction amplitude is obtained by solving a Lippmann-Schwinger type scattering equation for the interaction potential. The features of the $\bar{D}N$ amplitude based on this model are much more realistic than the ones employed in previous studies [22–24]. Indeed, in the former studies the D^-p cross section for instance was assumed to be momentum independent and equal to $\simeq$20 mb [22,24] or 5 mb [23]. Moreover, the angular dependence of the elastic scattering was assumed to be either isotropic [22,24] or forward peaked [23], i.e. proportional to $\exp(bt)$, where t is the four momentum transfer squared, with a slope b=2 GeV^{-2}. The reason for such assumptions was the lack of any microscopic calculations of the $\bar{D}N$ scattering amplitude in those days.

To illustrate the differences between the previous calculations [22–24] and the results of Ref. [20] we show in Fig. 2 predictions for the $D^-n \to D^-n$, $D^-p \to D^-p$ and $D^-p \to \bar{D}^0n$ reaction cross sections as a function of the $\bar{D}$-meson momentum (lower axis) and the cm kinetic energy ϵ (upper axis). It is clear that the scattering cross sections for all channels depend significantly on the $\bar{D}$-meson momentum.

Note that the $\bar{D}N$ scattering amplitudes for the different reaction channels shown in Fig. 2 are related to the isospin basis used in Ref. [20] by

$$T_M(D^-n \to D^-n) = T_M(\bar{D}^0p \to \bar{D}^0p) = f_1, \quad (11)$$

$$T_M(D^-p \to D^-p) = T_M(\bar{D}^0n \to \bar{D}^0n) = \frac{1}{2}(f_0+f_1), \quad (12)$$

$$T_M(D^-p \to \bar{D}^0n) = \frac{1}{2}(f_1 - f_0), \quad (13)$$

where f_0 and f_1 are the isospin I=0 and I=1 amplitudes, respectively.

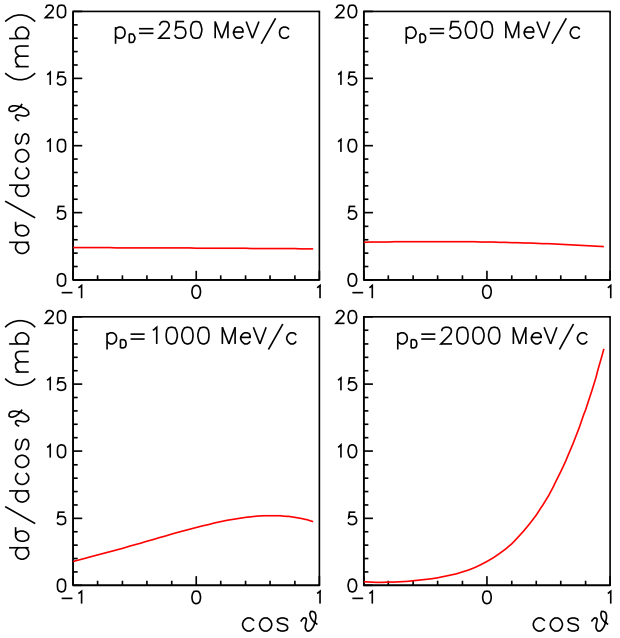

Fig. 3. Differential cross sections for the $D^-p \to D^-p$ reaction in the cm system at different momenta.

Differential cross sections for $D^-p \to D^-p$ at different momenta are presented in Fig. 3. The distributions are almost isotropic for momenta below $\simeq$500 MeV/c, but become forward peaked at higher momenta. Note that there is no simple way to parametrize the angular dependence with functions like $\exp(bt)$ [23], unless the slope parameter b is taken to be momentum dependent.

For completeness, let us mention that other models of the $\bar{D}N$ interaction have been published in recent years [41,49]. Those authors considered s-waves only. The cross sections predicted by these models at threshold are 8.5 mb ($D^-n \to D^-n$), 5.54 mb ($D^-p \to D^-p$), and 0.03 mb ($D^-p \to \bar{D}^0n$) [41,43] and 10.6 mb, 2.64 mb, and 2.64 mb for model B of Ref. [49], respectively.

3.2 The DN amplitude

The DN interaction [21] employed in the present study is also constructed in close analogy to the meson-exchange $\bar{K}N$ model of the Jülich group [50] as well as by exploiting the close connection between the $\bar{D}N$ and DN systems due to G-parity conservation. Specifically, the latter constraint fixes the contributions to the direct DN interaction potential while the former one provides the transitions to and interactions in channels that can couple to the DN system. Accordingly, the DN interaction is likewise provided by vector-meson (ρ, ω) exchange and higher-order box diagrams involving D^*N, $D\Delta$, and $D^*\Delta$ intermediate states. The short-ranged quark-gluon processes, however, are absent here because the quark-exchange mechanism cannot contribute to the DN interaction due to the different quark structure of the D meson. As far as the coupling to other channels is concerned, we follow here the arguments of Ref. [50] and we take into account only the channels $\pi\Lambda_c(2285)$ and $\pi\Sigma_c(2455)$. Furthermore, we restrict ourselves to vector-meson exchange and we do not consider any higher-order diagrams in those channels. Pole diagrams due to the $\Lambda_c(2285)$ and $\Sigma_c(2455)$ intermediate states are, however, consistently included in all channels.

In this basic model all free parameters - the coupling constants and the cut-off masses at the vertex form factors of the occurring meson-meson-meson and meson-baryon-baryon vertices, cf. [50] - are fixed by the assumed SU(4) symmetry and the connection with the $\bar{K}N$ model, respectively. When solving the coupled-channel Lippmann-Schwinger equation with this interaction model we observe that two states are generated dynamically below the DN threshold, one in the S_{01} partial wave and the other one in the S_{11} partial wave. (We use here the standard spectroscopical nomenclature $L_{I\,2J}$.) In view of the close analogy between our DN model and the corresponding $\bar{K}N$ interaction [50] this is not too surprising, because also the latter yields a quasi-bound state in the S_{01} channel which is associated with the $\Lambda(1405)$ resonance. The bound states in both the $\bar{K}N$ and DN are generated by the strongly attractive interaction due to the combined effect of ω, ρ and scalar-meson exchanges, which add up coherently in specific channels.

It should be said that studies of the $\bar{K}N$ and DN interaction within chiral unitary (and related) approaches likewise generate the $\Lambda(1405)$ resonance dynamically but also states in the DN system [41,44,51]. In those approaches the strong attraction is also provided by vector-meson exchange [41] or by the Weinberg-Tomazawa term [44,51]. In Refs. [42,44,49] the authors argued that the state occuring in the S_{01} channel of the charm $C = 1$ sector should be identified with the $I = 0$ resonance $\Lambda_c(2593)$. We adopt this viewpoint here too. Furthermore, we identify the state we get in the S_{11} channel with the $I = 1$ resonance $\Sigma_c(2800)$ [7].

In order to make sure that the DN model we are going to apply in our study of the reaction $\bar{p}d \to D^0D^-p$ incorporates these features also quantitatively we fine-tune the contributions of the scalar mesons to the DN interaction so that the position of those states generated by the model coincide with the values given in the list of the Particle Data Group. This can be achieved by a moderate change in the coupling constants of the σ meson (from 1 to 2.6) and the a_0 meson (from -2.6 to -4.6), cf. Table 2 in Ref. [20].

Interestingly, our model generates a further state, namely in the P_{01} partial wave, which, after the above fine-tuning, lies at 2803 MeV, i.e. just below the DN threshold. We are tempted to identfy this state with the $\Lambda_c(2765)$ resonance, whose quantum numbers are not yet established [7]. Though we do not reproduce the resonance energy quantitatively, we believe that further refinements in the DN model, specifically the inclusion of the $\Lambda_c\pi\pi$ channel in terms of an effective $\sigma\Lambda_c$ channel, can provide sufficient additional attraction for obtaining also quantitative agreement. The mechanism could be the same as in case of the Roper ($N^*(1440)$) resonance, which is generated dynamically in the Jülich πN model [52,53]. Here the required

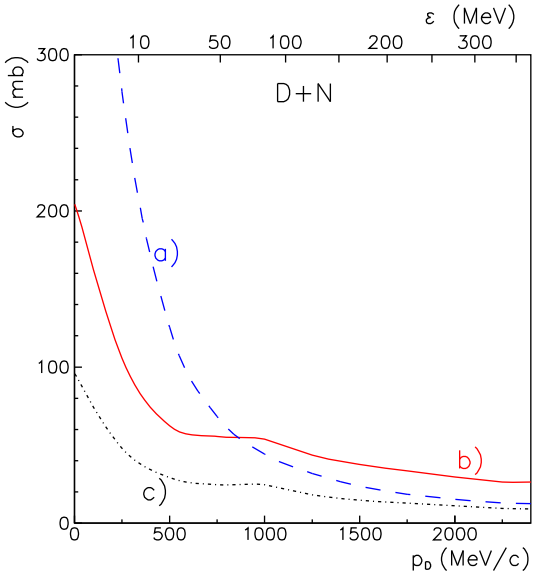

Fig. 4. Reaction cross sections for (a) $D^0n \to D^0n$ (dashed line), (b) $D^0p \to D^0p$ (solid line) and (c) $D^0p \to D^+n$ (dash-dotted line) as a function of the $\bar{D}$-meson momentum (lower axis) and the cms kinetic energy ϵ (upper axis).

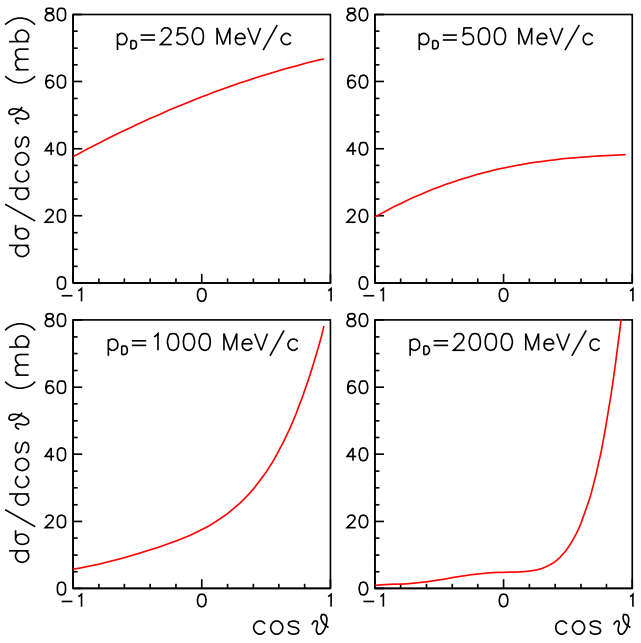

Fig. 5. Differential cross sections for the $D^0p \to D^0p$ reaction in the cm system at different momenta.

strong attraction is produced via the coupling of the πN p-wave (where the Roper occurs) to the s-wave in the σN system, facilitated by the different parities of the π and σ mesons.

Some results of our DN model are presented in Figs. 4 and 5. The DN scattering amplitude for the different reaction channels shown in the Fig. 4 are related to those in the isospin basis by

$$T_M(D^0n \to D^0n) = T_M(D^+p \to D^+p) = f_1, \quad (14)$$

$$T_M(D^0p \to D^0p) = T_M(D^+n \to D^+n) = \frac{1}{2}(f_0 + f_1), \quad (15)$$

$$T_M(D^0p \to \bar{D}^+n) = \frac{1}{2}(f_1 - f_0), \quad (16)$$

where f_0 and f_1 are the isospin I=0 and I=1 amplitudes respectively.

Obviously, also the DN cross sections show a significant momentum dependence in all charge channels. Furthermore, the cross sections are substantially larger than those we obtain for $\bar{D}N$. Specifically, for the pure $I = 1$ channel D^0n the cross section amounts to almost 600 mb at threshold. This is not too surprising in view of the nearby quasi-bound state. The latter is also reflected in the s-wave scattering lengths,

$$a_{DN}^{I=0} = (-0.41 + i0.04) \text{ fm}$$
$$a_{DN}^{I=1} = (-2.07 + i0.57) \text{ fm}, \quad (17)$$

namely by the rather large value of the real part in the $I = 1$ channel. For completeness, let us mention here that the scattering lengths of the DN interaction of Hofmann and Lutz [41], reported in [43], amount to about -0.4 fm for both isospin channels. In agreement with that work we find that the imaginary part is negligibly small for $I = 0$. However, contrary to [43] in our DN model this is not the case for the $I = 1$ channel.

Angular distributions for the reaction $D^0p \to D^0p$ are shown in Fig. 5. Obviously, there is a strong anisotropy already at fairly low momenta. It is due to significant contributions in the P_{01} partial wave in this momentum region induced by the near-threshold quasi-bound state produced by our model, as discussed above. For higher momenta the differential cross section becomes forward peaked, similar to the predictions of our model for the $\bar{D}N$ system.

Further details of our DN model will be reported in a forthcoming publication [21].

4 $\bar{D}D$ production in $\bar{p}N$ annihilation

The total cross section for the reaction $\bar{p}d \to D^0D^-p$ depends crucially on the elementary $\bar{N}N \to \bar{D}D$ annihilation amplitude T_A. Unfortunately, so far there is no experimental information about this reaction and even theoretical studies are rather scarce [54–56]. In Ref. [54] results were given for the reaction $\bar{p}p \to D^-D^+$ in a quark plus diquark model, where the elementary flavour changing process is due to diquark-antidiquark annihilation and subsequent creation of a quark-antiquark pair through one gluon. Kaidalov and Volkovitsky calculated the reaction $\bar{p}p \to \bar{D}D$ in the framework of a non-perturbative quark-gluon string model, based on secondary Regge pole exchanges including absorptive corrections [55]. The result of both works are summarized in Fig. 6. The larger cross sections are predicted by the model of Ref. [54] with a maximal value of around 0.15 μb at $p_{lab} = 12$ GeV/c corresponding to $\sqrt{s} \approx 5$ GeV. The model of Ref. [55] yields $\sigma_{\bar{p}p \to \bar{D}^0D^0} \approx 0.05$ μb at the maximum, while the one for $\bar{p}p \to \bar{D}^-D^+$ is a factor of 4 smaller. In both approaches, the unknown parameters of the models were fixed by considering corresponding flavour changing reactions involving strange quarks ($\bar{p}p \to \bar{K}K$ and/or $\bar{p}p \to \bar{\Lambda}\Lambda$, etc.).

Superficially the predictions of the two studies are qualitatively similar, specifically for $\bar{p}p \to \bar{D}^0D^0$ which in case of the model of Kroll et al. [54] is suppressed by roughly a factor four as compared to the prediction for $\bar{p}p \to D^-D^+$ [57] so that its maximal value would then practically coincide with the one obtained in [55]. However, for the reaction $\bar{p}p \to D^-D^+$ the magnitudes of the cross sections differ by more than a factor of 10. Furthermore, there is a significant difference in the energy dependence of the two model predictions, as seen in Fig. 6, so that the variations of the predictions are even larger in specific energy regions.

Admittedly, those results are only of limited use for our own investigation of the $\bar{p}d \to D^-D^0p$ reaction. For example, for the amplitude corresponding to the reaction chain $\bar{p}d \to D^-D^0p \to D^-D^0p$, involving rescattering in the $D^0p \to D^0p$ and $D^-p \to D^-p$ channels, one needs the pure $I = 1$ annihilation amplitude $\bar{p}n \to D^-D^0$ which cannot be reconstructed from the available information about those models. The other contributions to

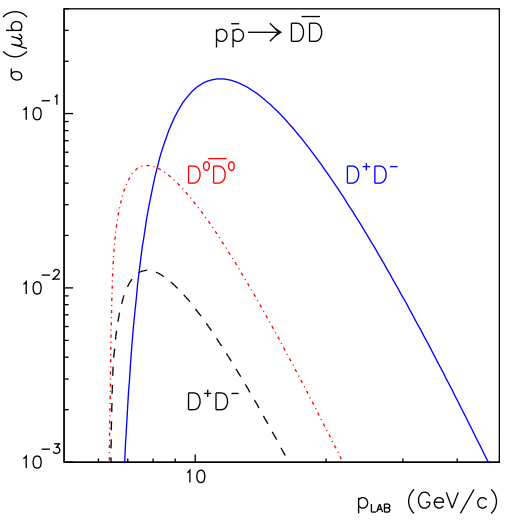

Fig. 6. Predictions for the $\bar{p}p \to \bar{D}D$ annhilation cross section taken from Refs. [54] (solid line) and [55] (dashed and dash-dotted lines).

the reaction amplitude, involving (DN or $\bar{D}N$) charge-exchange rescattering, $\bar{p}d \to D^-D^+n \to D^-D^0p$ and $\bar{p}d \to \bar{D}^0D^0n \to D^-D^0p$, require $\bar{p}p \to D^-D^+$ and $\bar{p}p \to \bar{D}^0D^0$, respectively, but here the relative phase between the terms is not known. Thus, we are facing the problem that we either have to add all contributions incoherently and make additional assumptions about the isospin dependence of $\bar{N}N \to \bar{D}D$ or we consider only the amplitude involving elastic DN and $\bar{D}N$ rescattering. We prefer the latter option. In this case we can add the Born term and the DN and $\bar{D}N$ rescattering contributions coherently, because they all involve the same elementary $\bar{p}n \to D^-D^0$ annihilation amplitude, and we can include the resulting interference effects in the evaluation of the observables. However, absolute predictions are out of reach and all results will be shown as number of events only. On the other hand we consider the energy dependence of the elementary $\bar{p}n \to D^-D^0$ annihilation amplitude in our calculation by adopting the results given in [55] for $\bar{p}p \to \bar{D}D$. But we should say that its influence on the observables shown in the present paper is practically negligible.

5 Open charm production in $\bar{p}d$ annihilation

Now we present results for D^0D^- production in antiproton-deuteron annihilation utilizing the formalism and the elementary DN and $\bar{D}N$ amplitudes described above, taking into account the Born diagram of Fig. 1a) and the rescattering diagram of Fig. 1b). For the latter we consider both D^-p and D^0p scattering in the final state. The $\bar{p}n \to D\bar{D}$ threshold on a free nucleon corresponds to the antiproton momentum of roughly 6.43 GeV/c. The absolute threshold for the $\bar{D}D$ production in antiproton-deuteron annihilation is at the antiproton momentum of 4.55 GeV/c. Evidently, close to the reaction threshold the production rate will be strongly suppressed by the phase space. We choose for our calculation the antiproton momentum of 7 GeV/c, corresponding to the region where the model calculation of [55] predicts the largest cross sections for the elementary $\bar{N}N \to \bar{D}D$ reaction.

5.1 Spectator momentum distribution

In Fig. 7 we present our predictions for the spectator proton momentum distribution. Here the solid histogram indicates the full result that includes the Born and the rescattering diagrams while the dashed line is the result based on the nucleon-exchange Born diagram alone, both obtained with the deuteron wave function of the CD Bonn NN potential [37]. Since the absolute normalization of the reaction cross section is quite uncertain we show the results as number of generated events.

The dotted and dash-dotted curves are results for the Born term alone employing the deuteron wave functions of the Paris [38] and full Bonn [39] potentials, respectively. Obviously, there is some model dependence which becomes more pronounced for spectator proton momenta above 300 MeV/c. But the rescattering mechanism is definitely by far the most dominant effect for momenta from around 400 MeV/c upwards. Since rescattering occurs in both D^-p and D^0p systems one needs to apply specific methods to separate their contributions in a reliable way, as will be discussed below.

In comparison to the multipion production case, cf. Figs. 11 and 12 in the Appendix, the enhancement due to the rescattering processes sets in at noticably higher spectator momenta and is also less pronounced. It was argued [25,26] that the strong enhancement seen in the proton

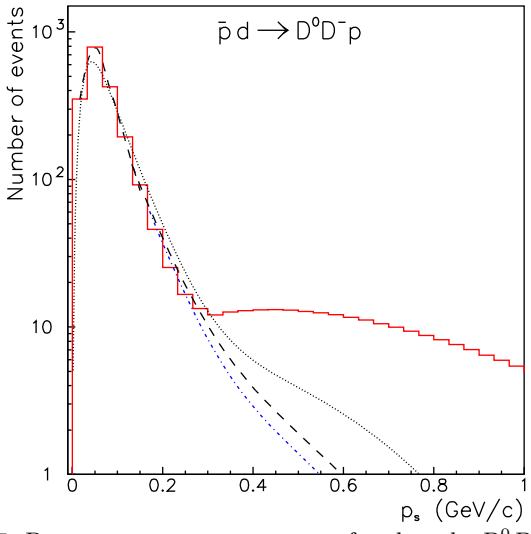

Fig. 7. Proton momentum spectrum for the $\bar{p}d \to D^0D^-p$ reaction. The dashed (dotted, dash-dotted) line shows the result of a calculation for the nucleon exchange Born diagram only (Eq. (2)) based on the s and d-wave parts of the deuteron wave function of the CD Bonn [37] (Paris [38], full Bonn [39]) NN potential. The solid histogram is the full calculation (for CD Bonn) that includes D^0p and D^-p rescattering.

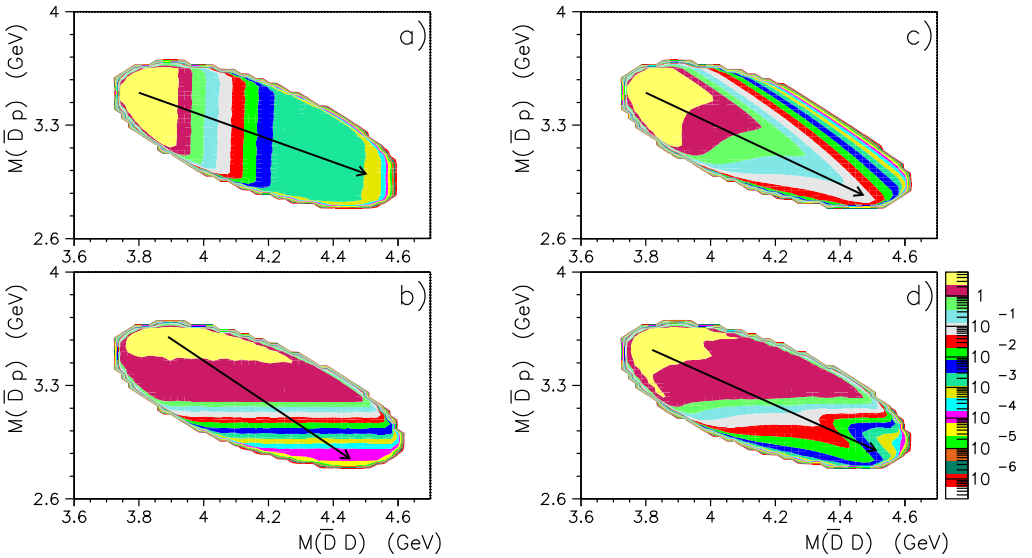

Fig. 8. Dalitz plot for the $\bar{p}d \to D^0 D^- p$ reaction. Here, $M(\bar{D}p)$ and $M(\bar{D}D)$ are the D^-p and D^0D^- invariant masses, respectively. The arrows points in the direction of decreasing intensity of the distribution. Each plot a)-d) is explained in the text.

momentum spectrum for the multipion reactions is to a good part due to the excitation of the $\Delta(1232)$ resonance in the πN rescattering processes. Though our DN scattering amplitude is dominated likewise by poles, in several partial waves, cf. the discussion above, their influence on the momentum spectrum seems to be smaller, presumably because they all lie below the DN elastic threshold. The enhancement we get for the $\bar{p}d \to D^0 D^- p$ reaction seems to be somewhat smaller than what was reported in an earlier model calculation by Cassing et al. [23]. But one has to keep in mind that in the latter work the contribution of the d-wave component to the Born (spectator) term was neglected and, moreover, the results for the Born term and the rescattering term are shown separately, while we added them coherently in our calculation.

5.2 Dalitz plot

A well-known method for the reconstruction of the reaction dynamics is the Dalitz plot analysis of the final state [33,58–61]. For instance, for multi-pion production from $\bar{p}d$ annihilation the presence of rescattering effects was demonstrated via the projection of the Dalitz plot on the invariant mass spectrum of the final πp system [32, 62]. An analysis in form of a partial wave decomposition of the Dalitz plot was proposed [58–60] for the $pp \to pK^+\Lambda$ reaction, which finally allowed to study and separate [61] non-resonant and resonant contributions in the $K^+\Lambda$ subsystem. A similar technique could be applied in the analysis of the $\bar{p}d \to D^0 D^- p$ reaction. This method allows to study all subsystems, D^0p, D^-p and D^0D^-, but obviously requires high mass resolution and significant statistics.

Fig. 8 presents the Dalitz plot evaluated for the reaction $\bar{p}d \to D^0 D^- p$ at the antiproton momentum of 7 GeV/c. The horizontal axes in the plot indicate the invariant mass of the D^0D^- system, while the vertical axes indicate the mass of the D^-p system. Here panel a) shows the results obtained with the nucleon-exchange Born diagram only, b) those obtained with D^-p rescattering alone, while c) illustrates the results with D^0p FSI alone. Finally, Fig. 8d) contains the full results, *i.e.* when all three contributions are included coherently. The arrows in the figures indicate the direction of decreasing intensity of the distribution. Note that we implemented a cut on the spectator proton momentum in the calculations in order to reduce the contribution from the Born diagram. Specifically, we considered only events involving spectator protons with momenta above 300 MeV/c.

Evidently, the differences between the distributions resulting from the different diagrams are quite significant. The result based on the Born term alone indicates strong correlations between the D^0- and D^--meson invariant mass. This is due to the fact that they are produced from the same vertex, namely via $\bar{p}n \to D^0 D^-$. The invariant energy of the D^0D^- system is essentially given by the energy of the incoming antiproton, while the dispersion of the distribution is related to the square of the deuteron wave function. Assuming the target neutron to be at rest, the invariant mass of the D^0D^- system produced in the reaction $\bar{p}n \to D^0 D^-$ at antiproton momentum of 7 GeV/c is equal to 3.86 GeV. The strong D^0D^- correlation produces also a kinematical reflection, detectable in the D^-p system, namely in form of an enhancement in the high mass D^-p spectrum. However, this enhancement, being purely kinematical, does not have any relevance for the interpretation of the rescattering mechanism.

Results obtained for the rescattering diagrams alone are shown in Figs. 8b) and c). It is clear that there are no strong correlations in the D^0D^- system anymore. Now the spectrum is primarily distorted by the corresponding rescattering terms. The D^-p and D^0p projections of the

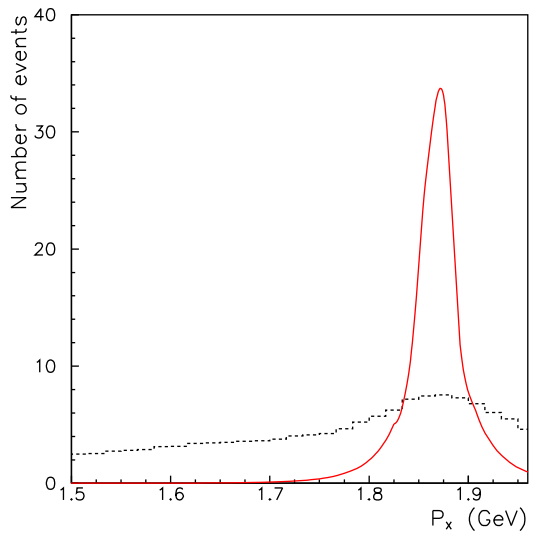

Fig. 9. The missing mass distribution of P_X given by Eq. (18) for the $\bar{p}d \to D^0 D^- p$ reaction. The dashed histogram shows results obtained with the nucleon-exchange Born diagram and the $D^0 p$ FSI for spectator proton momenta above 300 MeV/c. The solid histogram is the result for the $D^- p$ rescattering diagram based on Eq. (3).

Dalitz plot show the distribution produced by the relevant scattering amplitudes.

The final distribution, shown in Fig. 8d), corresponds to a calculation that includes the Born diagram plus both rescattering diagrams. It is fairly non-uniform and clearly indicates substructures resulting from the individual reaction mechanisms.

5.3 Missing mass of the exchanged meson

A method [63] that could be useful for the separation of the $\bar{D}N$ and DN rescattering contributions is based on the assumption that the dominant part of the rescattering amplitude comes from contributions where the particles in the intermediate state are on shell. We should emphasize that this method has no physical meaning when it comes to the off-shell part of the rescattering diagrams because then the exchanged meson is virtual.

Under the assumption that the charmed meson and nucleon are on-shell before undergoing rescattering, one can reconstruct the four-momentum of the meson in the loop following the missing mass technique via

$$P_X^2 = (P_s + P_{D^-} - P_N)^2, \qquad (18)$$

where P_s and P_{D^-} are the four-momenta of the spectator proton and the final D^- meson, and P_N is the four-momentum of the nucleon in the loop (i.e. the one involved in the rescattering process), given by the loop momentum q and energy E_q as in Eq. (3). Let us assume for the moment that the scattering process takes place on a free nucleon at rest. Then we would get $P_X^2 = m_D^2$, where m_D is the mass of the (incoming) D meson. However, since the reaction does not take place on a free nucleon but on a nucleon from the initial deuteron, the interacting nucleon is not at rest and, therefore, one expects a distribution of the missing mass in Eq. (18) around the central value of m_D reflecting the Fermi motion of the nucleon in the deuteron.

It is clear that the Born term as well as $D^0 p$ scattering would not lead to such a distribution because in this case there is no correlation between the four-momenta in Eq. (18).

In Fig. 9 we present results for the missing mass of the exchanged meson as given by Eq. (18), obtained for the antiproton momentum of 7 GeV/c. In the corresponding calculations the Born diagram and the rescattering amplitudes according to Eq. (3) are taken into account. Then we evaluate Eq. (18) using the four-momenta of the final spectator proton and of the final D^--meson, and assume that $P_N = (m_p, \mathbf{0})$. The dashed histogram in Fig. 9 includes contributions from the nucleon-exchange Born diagram for spectator momenta above 300 MeV/c as well as from the $D^0 p$ FSI. The solid histogram is the result obtained for the $D^- p$ rescattering term.

The results shown in the Fig. 9 look very promising with regard to the possibility for a separation of the reaction mechanisms. However, one should keep in mind that there are uncertainties due to the on-shell assumption made in the model calculation as well as in the evaluation of the missing mass, which cannot be quantified easily. Nonetheless, we want to mention that this method was actually used in Ref. [63] in the data evaluation and reconstruction of the hyperon production mechanisms in antiproton annihilation on xenon nuclei. Recently, this missing-mass method was also utilized for the analysis of K^+K^- pair production from carbon [64]. It is important to stress that the method cannot and should not be applied for too high momenta of the spectator proton, where the reaction is dominated by off-shell contributions and, therefore, the basic assumptions of the method are evidently no longer valid.

We have also performed calculations of the missing mass distribution for the corresponding case of a final D^0 meson where one can isolate the $D^0 p$ rescattering contributions. The results are qualitatively very similar to the D^- case and therefore we do not show them here.

5.4 Correlation between the scattering planes

Finally, we discuss the correlation between the two scattering planes [65]. One plane is given by the momenta of the antiproton and of the spectator proton. The other one is fixed by the momenta of the antiproton and of the produced charmed meson, the D^- meson, say. Then, due to the conservation of the transverse momenta in the $D^- p \to D^- p$ scattering process the azimuthal angle between these planes is peaked around $\phi \simeq 180°$. This correlation simply follows from the reaction kinematics. If the spectator proton is at rest before the scattering and the D^--meson has no transverse momentum, then, after

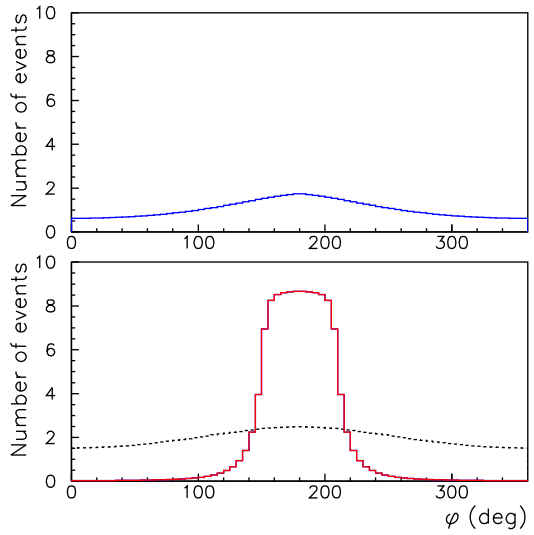

Fig. 10. The distribution of the azimuthal angle between the scattering plane given by the momenta of the antiproton and spectator proton and the plane fixed by the momenta of the antiproton and the D^--meson. The results are for spectator protons with momenta above 300 MeV/c. The upper panel shows the result for the Born diagram alone, while in the lower panel calculations including the D^-p and D^0p rescattering diagrams are presented. Here the solid histogram shows the distribution obtained for rescattering of the D^--meson, while the dashed histogram is the corresponding result for rescattering of the D^0-meson.

$D^-p \to D^-p$ scattering the transverse components of the momenta of the final D^--meson and proton must be exactly the same but aligned in opposite direction. However, both the Fermi motion in the deuteron and the $\bar{p}n \to D^-D^0$ annihilation allow for some variations in the transverse momenta of the spectator proton and of the D^--meson. That is why in an actual experiment one would expect a distribution of the azimuthal angle around the value ϕ=180°.

Results of our model calculation for the distribution of the azimuthal angle are presented in Fig. 10. They are obtained again by imposing a cut on the spectator proton momentum so that only momenta above 300 MeV/c contribute. The scattering plane is fixed by the momenta of the antiproton and the D^--meson. The upper panel of Fig. 10 shows predictions for the nucleon-exchange Born diagram while the lower panel contains results including the rescattering diagrams. Here the solid histogram corresponds to the contributions of the D^-p rescattering diagram and the dashed histogram to those from D^0p rescattering. From these results it seems feasible that the two rescattering contributions can be well isolated.

Also here we have considered the corresponding case for the D^0 meson, where again the results turned out to be qualitatively similar.

6 Summary

In this paper we examined the possibility to extract information about the DN and $\bar{D}N$ interactions from the $\bar{p}d \to D^0D^-p$ reaction. We utilized the notion that those open-charm mesons are first produced by annihilating antiprotons on the deuteron and subsequently rescatter on the remaining (spectator) nucleon. The latter process is then exploited for investigating the DN and $\bar{D}N$ interactions. To explore the potential of a corresponding experiment we performed concrete model calculations taking into account the nucleon-exchange Born diagram as well as rescattering diagrams.

As a test of the approach we first applied it to multipion production in $\bar{p}d$ annihilation and we compared our results with data available for the $\bar{p}d \to \pi^+2\pi^-p$ and $\bar{p}d \to 2\pi^+3\pi^-p$ reactions. These data [66–68] show strong evidence for contributions from $\pi N \to \pi N$ rescattering, which can be seen in the spectra of the spectator proton and invariant mass distribution of the final pion and proton. We obtained very reasonable agreement with the data available for the spectator proton distributions.

In our investigation of the $\bar{p}d \to D^0D^-p$ reaction we utilized realistic $\bar{D}N \to \bar{D}N$ [20] and $DN \to DN$ [21] scattering amplitudes. This is a substantial improvement over previous studies [22–24] which employed simplistic $\bar{D}N$ and DN scattering amplitudes based on somewhat questionable assumptions.

We found that below spectator momenta of around 300 MeV/c the reaction is dominated by the nucleon-exchange Born diagram. For higher spectator momenta there is a sizable contribution from the rescattering diagrams. In particular, their contribution is significantly larger than the uncertainties due variations in the high-momentum component of the deuteron wave function. Thus, selecting events with spectator momenta above 300 or 400 MeV/c, say, should allow to obtain a data sample that can be used for extracting information about the DN and $\bar{D}N$ interactions.

Subsequently we explored different methods for isolating the contributions from the DN and $\bar{D}N$ rescattering terms. We showed that the missing mass technique and the correlation between the planes given by the scattered meson and nucleon allow a reasonable reconstruction of the reaction dynamics and to separate the contributions of $\bar{D}N$ rescattering from those of DN rescattering. Since these methods are based on the reaction kinematics we consider them as promising tools to extract information on the $\bar{D}N$ and DN interactions from the reaction $\bar{p}d \to D^0D^-p$.

We appreciate discussions with A. Afanasev, W. Melnitchouk, W. Schweiger, S. Stepanyan, K. Tsushima and B. Wojtsekhowski. This work was financially supported by the Deutsche Forschungsgemeinschaft (Project no. 444 BRA-113/14 and through funds provided by the SFB/TR 16 "Subnuclear Structure of Matter") and the Brazilian agencies CAPES, CNPq and FAPESP. It was also supported in part by the Helmholtz Association through funds provided to the virtual institute "Spin and strong QCD"

(VH-VI-231). This research is part of the EU Integrated Infrastructure Initiative Hadron Physics Project under contract number RII3-CT-2004-506078. A.S. acknowledges support by the JLab grant SURA-06-C0452 and the COSY FFE grant No. 41760632 (COSY-085).

A Multi-pion production in $\bar{p}d$ annihilation

To illustrate the applicability of the discussed formalism we consider experimental data available for the reactions $\bar{p}d \to 2\pi^+ 3\pi^- p$ and $\bar{p}d \to \pi^+ 2\pi^- p$ obtained at the Low Energy Antiproton Ring (LEAR) at CERN using annihilation at rest in a hydrogen gas [66,67] and at the Brookhaven National Laboratory (BNL) using the deuterium bubble chamber [68].

We calculate the proton spectator distribution by summing the Born and rescattering amplitudes and integrating over the 6-body and 4-body final states. The calculations are done with the deuteron wave function of the CD-Bonn potential [37]. Available data [69,70] on pion multiplicities for $\bar{p}p$ annihilation at rest and in flight show practically no dependence on the antiproton momentum within the range up to $\simeq$100 MeV/c. Therefore, we assume the annihilation amplitude T_A to be a constant. The spectator proton momentum distribution was measured in different experiments [66–68] and the data were published with arbitrary normalization depending on the total number of detected events. Therefore, we normalize our calculation to the data but we also normalize the different data sets to each other, as explained below.

For evaluating the contribution from pion-nucleon rescattering we use the current solution of the GWU/CNS partial wave analysis [71,72]. We account for isospin and topological factors following the prescription given in Refs. [30,31,35]. The phase-space integration is done by the Monte-Carlo method based on event-by-event simulations. This allows us to apply kinematical cuts on the final pion momenta similar to that discussed in Refs. [66, 67] in order to investigate discrepancies between the data at spectator proton momenta below 250 MeV/c. We will come back to this issue later.

Experimental results for the proton momentum distribution for the reaction $\bar{p}d \to 2\pi^+ 3\pi^- p$ are shown in Fig. 11. The squares [66] and circles [67] are data from the LEAR facility while the triangles are from an experiment [68] at the Brookhaven National Laboratory (BNL) using the deuterium bubble chamber.

The basic difficulty in the counter measurements [66, 67] is the reconstruction of the low-momentum part of the spectator spectra. As mentioned in Ref. [66], for the direct proton detection at least transverse proton momenta of 130 MeV/c are required. The very low momentum protons can be only reconstructed through exclusive measurements of the final pions and applying the missing momentum method. But such a reconstruction introduces additional uncertainties in the low momentum spectator spectra. To avoid any ambiguity we normalized all data sets at momenta around 400 MeV/c, i.e. at values where the proton spectator momentum was measured directly. This normalization emphasizes that the shape of the measured spectrum from the different experiments is almost identical at higher spectator proton momenta. On the other hand, we see a substantial disagreement between the available data [66–68] at momenta below $\simeq$ 250 MeV/c.

Experimental results for the reaction $\bar{p}d \to \pi^+ 2\pi^- p$ are presented in Fig. 12. Again, the squares are LEAR data [66] while the triangles are from the BNL [68]. Both data sets are normalized at proton momenta around 400 MeV/c and in such a way that the scale is roughly the same as in Fig. 11. This allows us to compare the shapes of the spectator proton distributions for the two reactions. There is clearly a difference between those shapes for $\bar{p}d \to 2\pi^+ 3\pi^- p$ and $\bar{p}d \to \pi^+ 2\pi^- p$. Indeed one expects that the shape of the spectator momentum distribution depends on the momentum carried by the scattering meson and, consequently, that reactions with different final pion multiplicity would exhibit different shapes of the proton spectra. The more energetic pions from the $\bar{p}d \to \pi^+ 2\pi^- p$ reaction produce more energetic spectator protons in the rescattering. Qualitatively this follows from the rescattering amplitude of Eq. (3).

Again, for $\bar{p}d \to \pi^+ 2\pi^- p$ the experimental results are consistent at proton momenta above 250 MeV/c and disagree substantially at low momenta. As already indicated above, we applied kinematical cuts on the final pion momenta, similar to those discussed in Refs. [66,67], in the course of our investigation for the reaction $\bar{p}d \to \pi^+ 2\pi^- p$ as well as for $\bar{p}d \to 2\pi^+ 3\pi^- p$. But it turned out that those cuts do not resolve the disagreement between the data [66–68] at spectator proton momenta below 250 MeV/c.

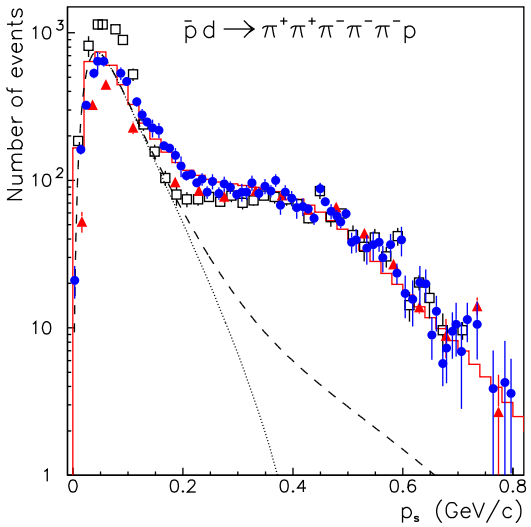

Fig. 11. Proton momentum spectrum for the $\bar{p}d \to 2\pi^+ 3\pi^- p$ reaction. The data are from Refs. [66] (squares), [67] (circles) and [68] (triangles). The dashed line shows the result from Eq. (2) taking into account s- and d-wave parts of the deuteron wave function while the dotted line is based on the s-wave component alone. The solid histogram is the full calculation including the nucleon exchange Born diagram and rescattering diagrams using the GWU/CNS πN partial-wave amplitudes [71,72] for T_M.

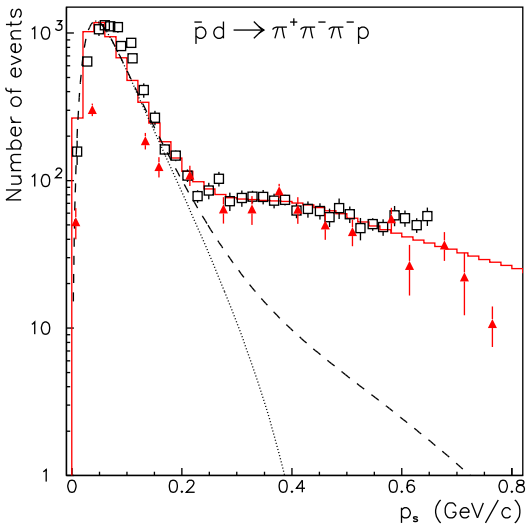

Fig. 12. Proton momentum spectrum for the $\bar{p}d \to \pi^+ 2\pi^- p$ reaction. The data are from Ref. [66] (squares) and [68] (triangles). Same description of curves as in Fig. 11.

Let us now come to the results of our model calculation and first discuss the normalization, which is a somewhat delicate issue. From a theoretical point of view it should be done preferrably around the peak in the distribution at low momenta where the spectrum is dominated by the Born diagram and the s-wave component of the deuteron wave function. But this is exactly the region where the experimental uncertainty is very large. Thus, we decided to normalize our results also in the plateau region, i.e. around 400 MeV/c. Note that the normalization is done for the full calculation. The relative size of the momentum distribution at the peak as compared to the plateau is fixed by the ingredients of the model alone, i.e. the contributions of the Born diagram and from the rescattering diagram. There is no additional normalization constant involved here.

The dashed lines in Figs. 11 and 12 correspond to the contribution from the nucleon-exchange Born diagram given by Eq. (2). Interestingly, our predictions for low momenta agree well with the data of [67] (for $\bar{p}d \to 2\pi^+ 3\pi^- p$) and [66] (for $\bar{p}d \to \pi^+ 2\pi^- p$). For proton momenta above 200 MeV/c all data show a substantial enhancement with respect to the predictions based on the Born term alone. For illustration purposes we show here also results using only the s-wave part of the deuteron wave function (dotted line). There have been some speculations that the enhancement at higher momenta could indicate an excitation of the short range component of the deuteron wave function [73–77]. But, in any case, a simple renormalization of the d-wave contribution would not reproduce the observed shape of the spectator proton distribution around the plateau, i.e. for $p_s \simeq 400$ MeV/c.

The solid histograms in Figs. 11 and 12 are the results of our full calculation including the nucleon-exchange Born diagram and the rescattering diagram. But we should say that the off-shell corrections of Eq. (6), not considered in the present investigation, are known to lead to variations of the order of 30% or more in the absolute value of the rescattering contribution, though they do not effect the shape of the spectator proton distribution [31].

Our results are in reasonable agreement with that of Ref. [31], but are in contradiction to the conclusions of Ref. [78], where the spectator proton momentum distribution is well reproduced by taking into account the Born diagram of Fig. 1a) and pion absorption on the spectator nucleon. However, there is strong experimental evidence in favor of the rescattering mechanism: The invariant mass spectrum of the $2\pi^+ 2\pi^-$ system from the $\bar{p}d \to 2\pi^+ 3\pi^- p$ reaction was measured [67] for different cuts on the spectator proton momenta. If the final pions do not undergo rescattering, such cuts should not change the invariant mass distribution. But in the experiment it turned out that the $2\pi^+ 2\pi^-$ invariant mass distribution depends substantially on the proton momentum cut when taken below or above $p_s = 200$ MeV/c.

References

1. T. Matsui and H. Satz, Phys. Lett. B **178**, 416 (1986).
2. H. Satz, J. Phys. G **32**, R25 (2006) [arXiv:hep-ph/0512217].
3. S. Batsouli, S. Kelly, M. Gyulassy and J.L. Nagle, Phys. Lett. B **557**, 26 (2003) [arXiv:nucl-th/0212068].
4. M. Djordjevic and M. Gyulassy, Phys. Lett. B **560**, 37 (2003) [arXiv:nucl-th/0302069].
5. N. Armesto, C.A. Salgado and U.A. Wiedemann, Phys. Rev. D **69**, 114003 (2004) [arXiv:hep-ph/0312106].
6. M. Djordjevic and M. Gyulassy, Nucl. Phys. A **733**, 265 (2004) [arXiv:nucl-th/0310076].
7. W.-M. Yao *et al.* [Particle Data Group], J. Phys. G **33**, 1 (2006)
8. G.D. Moore and D. Teaney, Phys. Rev. C **71**, 064904 (2005) [arXiv:hep-ph/0412346].
9. H. van Hees and R. Rapp, Phys. Rev. C **71**, 034907 (2005) [arXiv:nucl-th/0412015].
10. H. van Hees, V. Greco and R. Rapp, Phys. Rev. C **73**, 034913 (2006) [arXiv:nucl-th/0508055
11. S. Wicks, M. Djordjevic, C. Horowitz and M. Gyulassy, Nucl. Phys. A **784**, 426 (2007) [arXiv:nucl-th/0512076].
12. S.S.Adler *et al.* [PHENIX Collaboration], Phys. Rev. Lett. **94**, 082301 (2005)[arXiv:nucl-ex/0409028].
13. J. Bielcik *et al.* [STAR Collaboration], Nucl. Phys. A **774**, 697 (2006) [arXiv:nucl-ex/0511005].
14. Y. Zhang *et al.* [STAR Collaboration], J. Phys. G **32**, S529 (2006) [arXiv:nucl-ex/0607011].
15. C. Zhong *et al.* [STAR Collaboration], J. Phys. G **34**, S741 (2007) [arXiv:nucl-ex/0702014].
16. M. Kotulla et al., *Technical Progress Report for $\bar{P}$ANDA, Strong Interaction Studies with Antiprotons*, February 2005, http://www-panda.gsi.de/db/papersDB/PC19-050217_panda_tpr.pdf.
17. O.N. Hartmann *et al.* [PANDA Collaboration], Int. J. Mod. Phys. A **22**, 578 (2007).
18. K.T. Brinkmann, P. Gianotti, I. Lehmann [PANDA Collaboration], Nucl. Phys. News **16**, 15 (2006) [arXiv:physics/0701090].
19. W. Kuhn [PANDA Collaboration], Acta Phys. Polon. B **37**, 129 (2006).

20. J. Haidenbauer, G. Krein, Ulf-G. Meißner and A. Sibirtsev, Eur. Phys. J. A **33**, 107 (2007) [arXiv:nucl-th/0704.3668].
21. J. Haidenbauer et al., in preparation.
22. A. Sibirtsev, K. Tsushima and A. W. Thomas, Eur. Phys. J. A **6**, 351 (1999) [arXiv:nucl-th/9904016].
23. W. Cassing, Y. S. Golubeva and L. A. Kondratyuk, Eur. Phys. J. A **7**, 279 (2000) [arXiv:nucl-th/9911026].
24. A. Sibirtsev, Nucl. Phys. A **680**, 274c (2001).
25. C.G. Fasano and M.P. Locher, Z. Phys. A **336**, 469 (1990).
26. V.M. Kolybasov, I.S. Shapiro and Yu.N. Sokolskikh, Phys. Lett. B **222**, 135 (1989).
27. J.M. Laget, Phys. Rept. **69**, 1 (1981).
28. C.G. Fasano and M.P. Locher, Z. Phys. A **338**, 197 (1991).
29. J.M. Laget, Nucl. Phys. A **296**, 388 (1978).
30. M.P. Locher and B.S. Zou, Z. Phys. A **340**, 187 (1991).
31. C.G. Fasano, M.P. Locher and S. Nozawa, Z. Phys. A **338**, 95 (1991).
32. D.V. Voronov and V.M. Kolybasov, JETP Lett. **57**, 162 (1993).
33. E. Byckling and K. Kajantie, Particle Kinematics (Wiley and Sons, New York, 1973).
34. J.M. Laget, Phys. Rev. C **73**, 044003 (2006).
35. M.P. Locher and B.S. Zou, J. Phys. G **19**, 463 (1993).
36. J.M. Laget, Phys. Rev. C **75**, 014002 (2007) [arXiv:nucl-th/0603009].
37. R. Machleidt, Phys. Rev. C **63**, 024001 (2001) [arXiv:nucl-th/0006014].
38. M. Lacombe, B. Loiseau, J. M. Richard, R. Vinh Mau, J. Cote, P. Pires and R. De Tourreil, Phys. Rev. C **21**, 861 (1980).
39. R. Machleidt, K. Holinde, and Ch. Elster, Phys. Rept. **149**, 1 (1987).
40. Z. w. Lin, C. M. Ko and B. Zhang, Phys. Rev. C **61**, 024904 (2000) [arXiv:nucl-th/9905003].
41. J. Hofmann and M. F. M. Lutz, Nucl. Phys. A **763**, 90 (2005) [arXiv:hep-ph/0507071].
42. L. Tolos, J. Schaffner-Bielich and A. Mishra, Phys. Rev. C **70**, 025203 (2004) [arXiv:nucl-th/0404064].
43. M. F. M. Lutz and C. L. Korpa, Phys. Lett. B **633**, 43 (2006) [arXiv:nucl-th/0510006].
44. T. Mizutani and A. Ramos, Phys. Rev. C **74**, 065201 (2006) [arXiv:hep-ph/0607257].
45. R. Büttgen, K. Holinde, A. Müller–Groeling, J. Speth, and P. Wyborny, Nucl. Phys. A **506**, 586 (1990).
46. M. Hoffmann, J.W. Durso, K. Holinde, B.C. Pearce, and J. Speth, Nucl. Phys. A **593**, 341 (1995).
47. D. Hadjimichef, J. Haidenbauer and G. Krein, Phys. Rev. C **66**, 055214 (2002) [arXiv:nucl-th/0209026].
48. J. Haidenbauer and G. Krein, Phys. Rev. C **68**, 052201 (2003) [arXiv:hep-ph/0309243].
49. L. Tolos, A. Ramos and T. Mizutani, Phys. Rev. C **77**, 015207 (2008) [arXiv:0710.2684 [nucl-th]].
50. A. Müller-Groehling, K. Holinde, and J. Speth, Nucl. Phys. A **513**, 557 (1990).
51. M. F. M. Lutz and E. E. Kolomeitsev, Nucl. Phys. A **730**, 110 (2004) [arXiv:hep-ph/0307233].
52. O. Krehl, C. Hanhart, S. Krewald and J. Speth, Phys. Rev. C **62**, 025207 (2000) [arXiv:nucl-th/9911080].
53. A. M. Gasparyan, J. Haidenbauer, C. Hanhart and J. Speth, Phys. Rev. C **68**, 045207 (2003) [arXiv:nucl-th/0307072].
54. P. Kroll, B. Quadder and W. Schweiger, Nucl. Phys. B **316**, 373 (1989).
55. A. B. Kaidalov and P. E. Volkovitsky, Z. Phys. C **63**, 517 (1994).
56. B. Kerbikov and D. Kharzeev, Phys. Rev. D **51**, 6103 (1995) [arXiv:hep-ph/9408378].
57. W. Schweiger, private communication.
58. C. Hanhart, Phys. Rept. **397**, 155 (2004) [arXiv:hep-ph/0311341].
59. A. Sibirtsev, J. Haidenbauer, H.-W. Hammer and S. Krewald, Eur. Phys. J. A **27**, 269 (2006) [arXiv:nucl-th/0512059].
60. A. Sibirtsev, J. Haidenbauer, U.-G. Meißner Phys. Rev. Lett. **98**, 039101 (2007) [arXiv:hep-ph/0607212].
61. S. Abdel-Samad *et al.* [COSY-TOF Collaboration] Phys. Lett. B **632**, 27 (2006).
62. A. Sibirtsev, K. Tsushima and A. Faessler, Z. Phys. A **354**, 215 (1996) [arXiv:nucl-th/9511008].
63. V.V. Barmin *et al.* [DIANA Collaboration], Nucl. Phys. A **683**, 305 (2001).
64. M. Hartmann, Yu. Kiselev *et al.* [ANKE Collaboration], COSY Proposal **147**.
65. Y.S. Golubeva, W. Cassing, L.A. Kondratyuk, A. Sibirtsev and M. Büscher, Eur. Phys. J. A **7**, (2000) [arXiv:nucl-th/9910028].
66. J. Riedlberger *et al.*, Phys. Rev. C **40**, 2717 (1989).
67. S. Ahmad *et al.*, IVth LEAR Workshop: Physics at LEAR with Low-Energy Antiprotons, Villars-sur-Ollon, Switzerland (1987), edited by C. Amsler *et al.*, Nucl. Sci. Res. Conf. Ser. **14**, 447 (1988).
68. P.D. Zemany, Z.M. Ma and J.M. Mountz, Phys. Rev. Lett. **38**, 1443 (1977).
69. J. Vandermeulen, Z. Phys. C **37**, 563 (1988).
70. C. Amsler, Rev. Mod. Phys. **70**, 1293 (1998) [arXiv:hep-ex/9708025].
71. R.A. Arndt, I.I. Strakovsky and R.L. Workman Phys. Rev. C **52**, 2120 (1995) [arXiv:nucl-th/9505040].
72. R.A. Arndt, W.J. Briscoe, I.I. Strakovsky and R.L. Workman, Phys. Rev. C **74**, 045205 (2006) [arXiv:nucl-th/0605082].
73. P. Benz and P. Söding, Phys. Lett. B **52**, 367 (1974).
74. P.J. Mulders and A.W. Thomas, Phys. Rev. Lett. **52**, 1199 (1984).
75. Y.E. Kim and M. Orlowski, Phys. Rev. C **29**, 2299 (1984).
76. L.Ya. Glozman, Prog. Part. Nucl. Phys. **34** 123 (1995).
77. L.-C.Lu and T.-S. Cheng, Phys. Lett. B **386**, 69 (1996).
78. A.E. Kudryavtsev and V.E. Tarasov, Sov. J. Nucl. Phys. **54**, 36 (1991).